

# Reconstruction of Storage Ring's Linear Optics with Bayesian Inference

Yue Hao,<sup>1</sup> Yongjun Li,<sup>2</sup> Michael Balcewicz,<sup>1</sup> Leo Neufcourt,<sup>1</sup> and Weixing Cheng<sup>2</sup>

<sup>1</sup>FRIB/NSCL, Michigan State University, East Lansing, MI 48864

<sup>2</sup>Brookhaven National Laboratory, Upton, NY 11973

A novel approach of accurately reconstructing storage ring's linear optics from turn-by-turn (TbT) data containing measurement error is introduced. This approach adopts a Bayesian inference based on the Markov Chain Monte-Carlo (MCMC) algorithm, which is widely used in data-driven discoveries. By assuming a preset accelerator model with unknown parameters, the inference process yields the their posterior distribution. This approach is demonstrated by inferring the linear optics Twiss parameters and their measurement uncertainties using a set of data measured at the National Synchrotron Light Source-II (NSLS-II) storage ring. Some critical effects, such as radiation damping rate, decoherence due to nonlinearity and chromaticity can also be included in the model and inferred. These effects are usually ignored in existing approaches. One advantage of the MCMC based Bayesian inference is that it doesn't require a large data pool, thus a complete optics reconstruction can be accomplished from a limited number of turns in a single data snapshot, before a significant machine drift can happen. The precise reconstruction of the parameter in accelerator model with the uncertainties is crucial prior information for applying the them to improve machine performance.

## I. INTRODUCTION

In accelerator operations, a significant amount of diagnostic data is recorded to understand the statistical properties of the bunched charge particles. The diagnostic data may be the first order moment (beam centroid) from beam position monitors (BPMs), second order moment (beam size) or sampling of the beam distribution from the projection on the various types of the profile monitors. These data are the only clue to tune the control knobs to make the accelerator as the machine we designed. Among all tuning tasks, the adjustment of linear optics is one of the most important task to improve the accelerator performance. A more detailed summary on linear optics measurements are reviewed in Ref.[1].

There are various established methods used to characterize the linear optics experimentally, using the Turn-by-Turn (TbT) BPM data of a storage ring. These includes independent component analysis (ICA)[2], model independent analysis (MIA)[3], and orthogonal decomposition analysis (ODA)[4] for retrieving the optics functions tunes, dispersions and chromaticities. Another well-developed and widely used method is linear optics from closed orbit (LOCO) [5], which heavily depends on the lattice model.

In this article, we demonstrate an alternative method to retrieve these machine properties using Bayesian Inference from BPMs' TbT data. Bayesian Inference is a powerful tool to infer unknown parameters  $\theta = (\theta_1, \theta_2, \dots, \theta_N)$  of a preset model from a measurement set  $M$ . In this method, we treat all to-be-inferred parameters as distribution functions with initial hypothesis  $H$ , described by its probability  $P(H)$ . Since the initial hypothesis is assumed before observing any measurement data, it is usually referred as prior probability. After considering the measurement set  $M$ , the probability of the hypothesis is modified, and becomes the posterior probability

$P(H | M)$ . Using the Bayes' theorem, we have

$$P(H | M) = \frac{P(M | H) \cdot P(H)}{P(M)} \quad (1)$$

here,  $P(M | H)$  is the possibility of the observing  $M$  assuming the hypothesis  $H$  is valid, also known as the likelihood function.  $P(M)$  is the marginal probability, which does not depend on the hypothesis  $H$ . Alternatively,  $P(M)$  can be interpreted as the normalization factor calculated from the integral of all possible hypothesis:

$$P(M) = \int P(M | H') dH' \quad (2)$$

Directly evaluating the Bayes' theorem is difficult, not only because the normalization factor in Eq. 2 usually cannot be integrated explicitly, but also due to the possible high dimension of the unknown parameter space. Therefore, we adopt the memoryless random step search routine, the Markov Chain Monte Carlo (MCMC) methods, to sample the posterior probability which is proportional to

$$P(H | M) \sim P(M | H) \cdot P(H) \quad (3)$$

without evaluating  $P(M)$ . The detailed algorithm of MCMC is introduced in Appendix. The structure of this article is outlined as below: we will detailed the betatron model and its parameters in the next chapter (chapter II), then illustrate the inference results of the optics function in chapter III, and discuss the model selection criteria for the Bayesian Inference in chapter IV.

The result of the Bayesian Inference, which is the sample from posterior distribution of the parameter in the model, can play an important role of refining the accelerator settings. In the optics inference example, as the readers will explore in the next chapters, the posterior

distribution of the Twiss parameters will be essential in the understanding of how well the optics correction can be achieved based on the measurement. Recently, a Bayesian approach [6] was studied for linear optics correction in a storage ring, i.e. given a set of measured linear optics distortions with some uncertainties, a prior distribution of quadrupole error can be used to specify an optimal regulation coefficient to prevent overfitting.

## II. MODEL AND MEASUREMENT DATA

Consider  $N$  BPMs distributed around a storage ring. These BPMs can record some selected bunches' [7] TbT trajectory for  $T$  turns after the beam is excited to perform a betatron oscillation. We can construct a betatron oscillation model to represent the measurement data without detailed knowledge of the accelerator, such as the layout of the lattice and the magnet strength. In general the Betatron motion recorded by the  $i^{\text{th}}$  BPM at  $j^{\text{th}}$  turn can be written as:

$$x_i(j) = x_{c,i} + A(j)x_i(0) \cos(2\pi\nu_x j + \phi_i) + \xi_i(j) \quad (4)$$

---


$$\begin{pmatrix} x_{\beta,i} \\ x'_{\beta,i} \end{pmatrix}_j = A(j) \begin{pmatrix} \cos 2\pi\nu_x + \alpha \sin 2\pi\nu_x & \beta \sin 2\pi\nu_x \\ -(1 + \alpha^2) \sin 2\pi\nu_x / \beta & \cos 2\pi\nu_x - \alpha \sin 2\pi\nu_x \end{pmatrix} \begin{pmatrix} x_{\beta,i} \\ x'_{\beta,i} \end{pmatrix}_0$$

Here we also assume that the decoherence and radiation damping effect are weak, so that, within same number of turns, the action of the particle  $J$  is conserved across all the BPMs. This assumption is valid for almost every existing hadron or electron storage ring. The action  $J$  has the form:

$$J_i(j) = \frac{1}{\beta} \left( x_{\beta}^2 + (\beta x'_{\beta} + \alpha x_{\beta})^2 \right) = C(j)$$

In this form, only information of  $x_{\beta}$  can be retrieved from BPM data, while  $\beta$ ,  $\alpha$  and  $x'_{\beta}$  are unknown. We can only infer the combination of these three unknowns. Following the usual accelerator physics notation, we will only infer the conjugate variable pair  $(x_{\beta}, P_x)$ , where the conjugate momentum  $P_x$  is:

$$P_x = \beta x'_{\beta} + \alpha x_{\beta}$$

then we can get

$$J\beta = x_{\beta}^2 + P_x^2 \quad (6)$$

Therefore we achieve the beta function at each BPM up to a constant  $J$ , which is assumed constant for all BPMs in one turn.

Here,  $x_{c,i}$  is the closed orbit at  $i^{\text{th}}$  BPM,  $\nu_x$  is the horizontal betatron tune and  $\phi_i$  is the phase constant at  $i^{\text{th}}$  BPM.  $A(j)$  is introduced to represent the envelope evolution due to decoherence and radiation damping effect, which will be addressed later. At each turn, the BPM reading contains a random error which follows the Gaussian distribution with a zero mean value and standard deviation  $\sigma_{\xi}$ .

We treat the first two terms in Eq. 4 as our 'model':

$$x_{i,model}(j) = x_{c,i} + A(j)x_i(0) \cos(2\pi\nu_x j + \phi_i) \quad (5)$$

Then the difference of the measurement data and the model follows a random Gaussian distribution:

$$x_{i,data} - x_{i,model} \sim N(0, \sigma_{xi})$$

for all  $j^{\text{th}}$  measurements. The Gaussian random distribution is centered at zero, because we cannot distinguish the bias of the BPM reading and the beam closed orbit  $x_{c,i}$ .

The betatron oscillation part of the model can be rewritten in terms of the Twiss parameters:

---

Finally, we have to choose a model to reflect obvious damping behavior and determine the factor  $A(j)$ . We choose to express the factor inside the exponential function as a polynomial of the turn number:

$$A(j) = \exp(-\epsilon_{SR}j - \epsilon_{NL}^2 j^2)$$

Clearly, we can link the coefficients  $\epsilon_{SR}$  and  $\epsilon_{NL}$  to the synchrotron radiation damping and nonlinear decoherence effect [8] respectively.

In this simplified model, we only include the transverse motion in one direction and excluded the effect of chromaticity. The treatment of synchrotron/transverse coupling will be discussed at the end of this article.

## BAYESIAN INFERENCE

The unknown parameters in the model (Eq. 5) are noted as  $\theta = (x_0, x_c, P_x, \nu_x, \epsilon_{SR}, \epsilon_{NL})$ , along with the standard deviation of the Gaussian distribution  $\sigma_{\xi}$ . These parameters will be inferred from the TbT data  $X_{data} = (x_0, x_1, \dots, x_{T-1})$ . Here, the data for each BPM in one measurement is  $\sim 2000$  turns. Applying

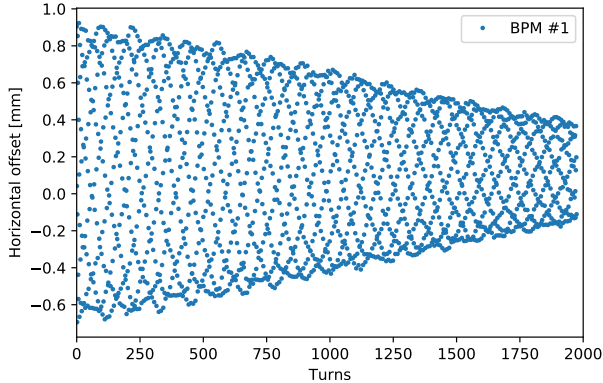


Figure 1. BPM reading of the first BPM

Table I. Initial values, step sizes and the inference results of parameters in the model Eq.5

	Initial values	Step sizes	Inference results
$x_0$ (mm)	$X_{data,0}$	$1 \times 10^{-3}$	$0.593 \pm 1.4 \times 10^{-3}$
$x_c$ (mm)	$\bar{X}_{data}$	$1 \times 10^{-3}$	$0.116 \pm 3.7 \times 10^{-4}$
$P_x$ (mm)	0	$1 \times 10^{-3}$	$-0.614 \pm 1.5 \times 10^{-3}$
$\nu_x$	Peak of DFT	$1 \times 10^{-7}$	$0.22055 \pm 2.7 \times 10^{-7}$
$\epsilon_{SR}$	0	$1 \times 10^{-6}$	$1.99 \times 10^{-4} \pm 6 \times 10^{-6}$
$\epsilon_{NL}$	0	$1 \times 10^{-6}$	$4.24 \times 10^{-4} \pm 4 \times 10^{-6}$
$\delta_\xi$ (mm)	$1 \times 10^{-3}$	$1 \times 10^{-3}$	$0.0164 \pm 2.7 \times 10^{-4}$

the Bayesian theorem (Eq. 3), we have:

$$P(\theta | X = X_{data}) \sim P(X = X_{data} | \theta) P(\theta)$$

which can be calculated using MCMC method.

We use a set of measured NSLS-II TbT data to demonstrate this method. The NSLS-II is a 3rd generation light source, which has 30 double bend achromat cells [9]. It is equipped 180 quasi-uniformly distributed BPMs for the purpose of orbit and lattice monitoring and control. The beam can be excited with a horizontal and a vertical fast pulse magnets to perform a free Betatron oscillation. The BPMs are configured with TbT resolution and having a gated functionality to lock on a selected diagnostic bunch train [7]. Figure 1 shows TbT data from one of these 180 BPMs.

The BPM reading reflects the orbit excursion, due to closed orbit, initial beam kick, the machine properties and the TbT reading errors. The BPM random error of one turn is independent from the measurement of other turns and assumed to be Gaussian random distribution. Therefore the likelihood  $P(X_{data} | \theta)$  can be expressed as:

$$P(X_{data} | \theta) \sim \exp\left(-\frac{1}{2\sigma_\xi^2} \sum_{j=0}^{T-1} (x_{data,j} - x_{model,j})^2\right)$$

The prior probability  $P(\theta)$  reflects our foreknowledge

of these parameters before the measurement. For example, we believe that the parameter  $x_0$  should be very close to the first value of measurement data  $x_{data,0}$ ; the closed orbit parameter should be close to the average value of the measurement  $\bar{X}_{data}$ , while the transverse tune  $\nu_x$  is expected to be close to the discrete Fourier transform (DFT) of the BPM data. In addition, the prior distribution can also be used to confine the range of the parameter, such as confining the parameter  $\epsilon_{SR}$  and  $\epsilon_{NL}$  to be positive. A proper prior will improve the MCMC convergence efficiency and conversely, an incorrect prior will bias the posterior distribution.

In this model, we do not imply any specific prior distribution other than requiring  $\epsilon_{SR}$  and  $\epsilon_{NL}$  to be positive. The initial value and the step size of each parameter is given in Table I. The initial value of each parameter reflects the ‘best-guess’ value for the corresponding parameter. The choice of the step size also plays an important role in the inference process. A too small step size would require long iteration steps and long computation time, while a too large step size will result in failure to reach convergence. A proper choice of the step size of one parameter should be smaller than the order of the uncertainty of the parameter. In this example, the step sizes of  $x_0$ ,  $x_c$ ,  $P_x$ ,  $\delta_\xi$  are set to 1 micron, based on a reasonable guess that the NSLS-II BPMs have TbT resolution around 10 microns. The proper step sizes of other parameters are determined by various trials with simulations.

Figure 2 and Figure 3 show the MCMC iterations for the data from one of the BPM. All figures illustrate convergence results after 25000 iterations. The parameter values of each iteration after convergence reaches (cyan shaded area in each figure) can be used to calculate the posterior distribution. The histogram can be plotted to represent the distribution and is attached to the right of each iteration plot. The converged results and their standard deviations are listed in the last column of Table I.

It is important to note that the uncertainties are obtained from one snapshot of data ( $\sim 2000$  turns) with the Bayesian inference. Comparing with other methods, such as ICA, MIA and ODA, each snapshot can only give one measurement result and the uncertainty must be obtained from repetitive measurements. However, the machine is continuously drifting during repetitive data collection. Therefore the uncertainty from repetitive measurement is over-estimated with the traditional methods. The overestimated uncertainty could potentially affect the ultimate performance of linear optics correction [6].

A notable feature of the inferred tune can be found in bottom left plot of Figure 2 and the inference result in I. The initial guess of the transverse tune from the peak DFT position of the BPM’s data is not precise enough due to a limited length of the data. The inferred tune has much higher accuracy ( $\sim 10^{-7}$  compared with  $\sim 1/T$ ,  $T$  is the number of turns). The high accuracy of the inferred tune using Bayesian Inference is because of fitting the data with the preset model, which is similar to the nu-

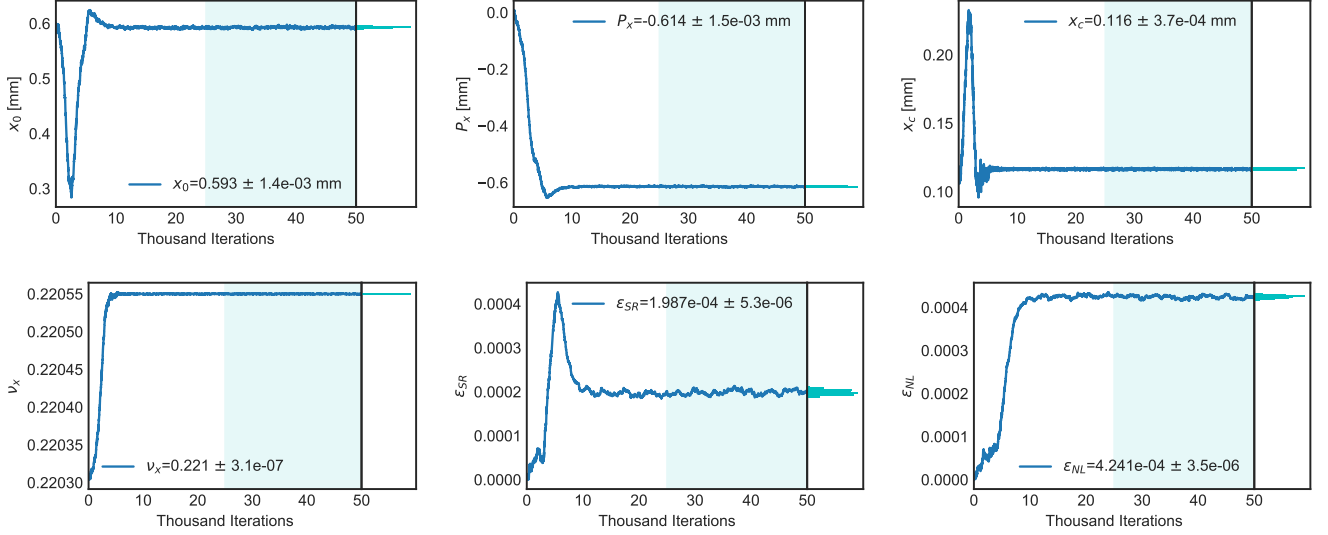


Figure 2. The MCMC iterations of parameter  $\theta$  using the measurement data of BPM #1. From left to right, the top figures are the iterations for  $x_0$ ,  $P_x$  and  $x_c$ ; the bottom figures are for  $v_x$ ,  $\epsilon_{SR}$  and  $\epsilon_{NL}$  respectively. A histogram plot is attached to the right of the each iteration plot. The histogram is taken from the second half of the total iteration, which is highlighted by the shaded area.

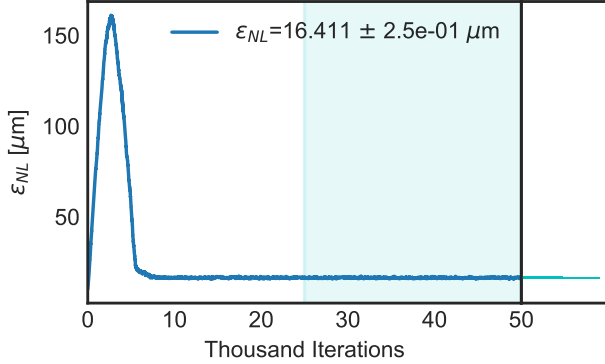


Figure 3. MCMC iteration of the width of the Gaussian error.

merical analysis of fundamental frequency (NAFF) [10] method. However, the NAFF method aims on searching for a single frequency oscillation, while Bayesian Inference achieves not only a precise tune, but also its uncertainty. In addition to the pure betatron oscillation, it is convenient to additional envelop profiles according to the physics, which is represented by the envelope factor  $A(j)$  in the our model. It is worthwhile to note that many form of envelope function will change the frequency of the oscillation, although the change may be small enough to neglect in real applications.

Figure 4 shows that the model with inferred parameter well represented the measurement data, with the difference plotted in orange dots. The difference is assumed as a Gaussian random number and is characterized by its standard deviation  $\sigma_\xi$ . However, our model is not

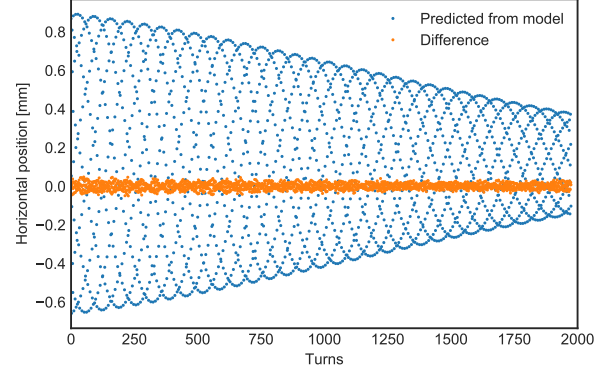


Figure 4. Reconstruction of the BPM #1 reading using model with inferred parameter (blue) and the difference with the measurement data (orange)

accurate enough to reflect all physics in the accelerator. The difference of the measurement data and the model prediction must contain other 'signals' rather than pure BPM noises. Therefore, the estimation of  $\sigma_\xi$  only gives a upper bound of the actual BPM noises. We can perform Fourier analysis on the difference data as shown in figure 5. Clearly we see the transverse coupling signal at a tune of about 0.26 as well as two synchrotron sidebands, about 0.009 away from the transverse tune 0.222.

As pointed out in the previous section, the initial position  $x_0$  and its conjugate momentum  $P_{x,0}$  can be inferred from the data. Then, as shown in Eq. 6, the beta function can be determined by up to a constant  $J$ , which is

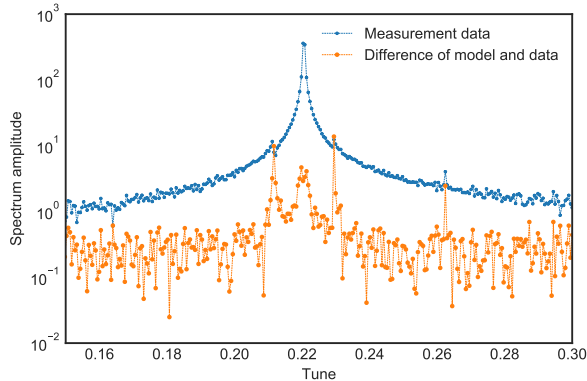


Figure 5. The frequency spectrum of measurement data of BPM #1 (blue points) and the difference between measurement and model with inferred parameters (orange points)

the action of the centroid of the beam and remain approximately constant for all BPMs within one turn. From the inference result of the first BPM, we can calculate:

$$\begin{aligned}\beta J &= (x_0 - x_c)^2 + P_x^2 \\ &= 0.602 \pm 0.003 \text{mm}^2\end{aligned}$$

We can repeat this inference for all BPMs and get the  $\beta J$ . However, we can not retrieve the constant  $J$  from the BPM datas. We have to choose a constant  $J$ , so that the average of the inferred beta function equals the average of the beta function, calculated from the accelerator model. This step of scaling only aims on producing inferred beta function in the familiar range. Figure 6 shows the inferred beta functions and its error bars, which is barely visible in this plotting scale. For better visibility, only beta function at first 90 BPM are plotted. The average standard deviation of beta function is about 0.47%. This measurement uncertainty can also be used directly to define the regularization coefficients in order to prevent overfitting issue, as pointed out in [6].

The betatron phase  $\phi_\beta$  is calculated as:

$$\phi_\beta = \arctan\left(\frac{P_x}{x_0 - x_c}\right)$$

Figure 7 compares the inferred betatron phase and the phase calculated from the accelerator model. The standard deviations of the betatron phase varies from  $1.5 \times 10^{-3}$  and  $3 \times 10^{-3}$  rad, therefore is not visible in the figure.

One necessary cross-check of the inference of all the BPMs is to check the parameters for the entire ring, which are  $\nu_x$ ,  $\epsilon_{SR}$  and  $\epsilon_{NL}$ . They are the 'integrating' parameters and reflects the dynamics of the entire ring. Figure 8 shows the inferred mean values of  $\nu_x$ ,  $\epsilon_{SR}$ , and  $\epsilon_{NL}$  from data of 180 BPMs, and their histograms are

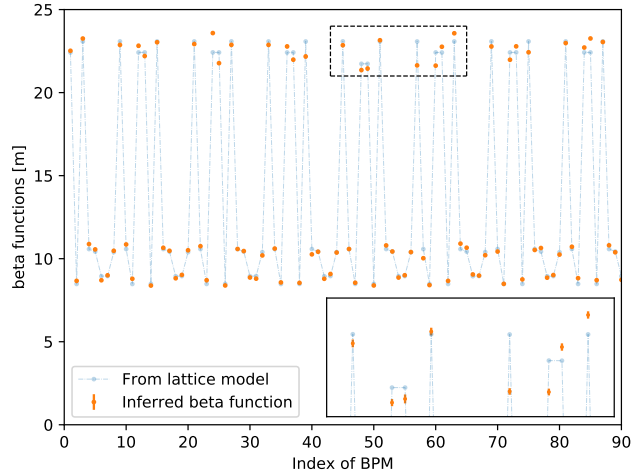


Figure 6. The inferred beta function at first 90 BPMs and its standard deviation error (orange dots), with the beta function calculated from bare lattice (in blue dotted lines) as a reference.

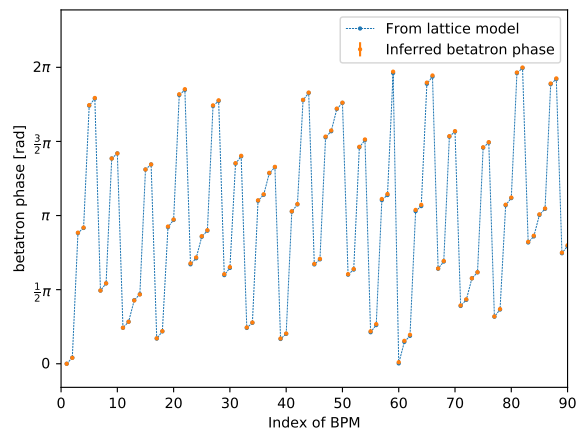


Figure 7. The inferred betatron phase at first 90 BPMs (orange dots), with the betatron phase advance calculated from bare lattice (blue dotted line) as reference. In both cases, the phases at first BPM are set to zero.

Table II. Comparison of standard deviation of the mean values of 180 inferences and the average of the standard deviation in each inference.

	Standard deviation of mean value of 180 inferences	Average of the uncertainty of each mean value
$\nu_x$	$1.9 \times 10^{-7}$	$3.4 \times 10^{-7}$
$\epsilon_{SR}$	$5.5 \times 10^{-6}$	$6.0 \times 10^{-6}$
$\epsilon_{NL}$	$3.6 \times 10^{-6}$	$4.1 \times 10^{-6}$

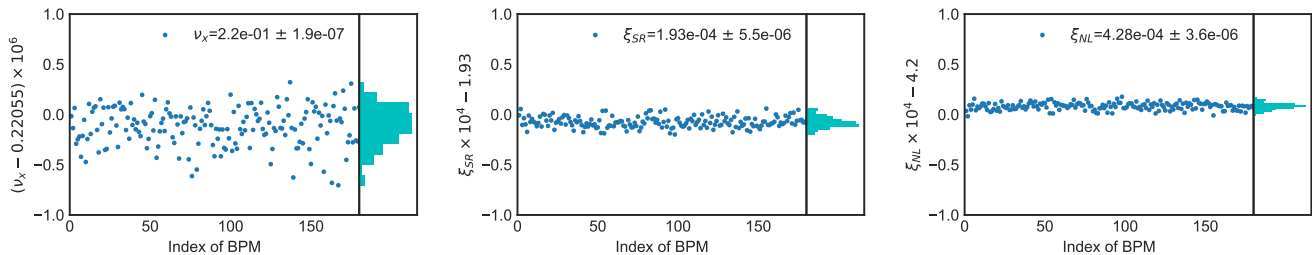


Figure 8. The tune,  $\epsilon_{SR}$  and  $\epsilon_{NL}$  inferred from all 180 BPMs. For easier reading, they are rescaled and shifted to the range  $[-1,1]$ . The quantity being plotted are left:  $(\nu_x - 0.22055) \times 10^6$ , middle:  $\epsilon_{SR} \times 10^4 - 1.93$  and right:  $\epsilon_{NL} \times 10^4 - 4.20$ .

attached to the right. Table II illustrates that the deviation of the mean values of the 180 inference results is less than the average of the uncertainty (standard deviation) of each mean value. It supports our belief that we can infer very similar values of  $\nu_x$ ,  $\epsilon_{SR}$ , and  $\epsilon_{NL}$  from all BPMs, as it should be from the physics behind the model. However, the samples of each BPM do not support that these mean values from each BPM are exactly the same in a statistical sense. It is expected because the model used in this chapter does not reflect all physics processes that the BPM records, than there is no guarantee that the ignored parts are orthogonal to the betatron motion that we infer.

## MODEL SELECTION

The results in the previous sections are based on the assumed model in Eq. 5. A valid model is the key to the success of Bayesian inference. The model itself can be also viewed as the strongest prior information, which prevents from treating the accelerator as a black box. The confidence of placing this model based on physics knowledge, instead of other general models such as artificial neural network, is based on the belief that the accelerator model is expected to represent most of the physics in the accelerator. In this chapter, we discuss the strategy of model selection in Bayesian Inference.

One could choose a very precise model with detailed accelerator elements such as the magnets, cavities and the drift space between them. The currents, voltage and the geometric information (length, distances) will be the unknown parameters to be inferred from measurement data. However, it is impractical to infer a high-dimensional problem, as there are usually thousands of knobs to describe the accelerator lattice to be inferred, even with a strong prior assumption and large amount of data. Meanwhile, in most cases, the goal of optimizing accelerator operation is not to know every detail of the accelerators, but the key parameters that affect the performance, for instance the beam behavior at the interaction point in colliders or at the insertion devices of synchrotron light sources.

Therefore it is reasonable to choose the model to represent

the interested dynamics with few parameters. In our example from the previous chapter, we focus only on betatron motion and its damping envelope, as in Eq. 5. In many existing methods, the damping envelope is ignored, which corresponds to adjusting our model by forcing  $A(j) \equiv 1$ . This reduces the model to

$$x_{i,model}(j) = x_{c,i} + x_i(0) \cos(2\pi\nu_x j + \phi_i) \quad (7)$$

where only four parameters  $\theta_{reduced} = (x_0, x_c, P_x, \nu_x)$  will be inferred. We refer to this model as 'reduced model' later. Using a smaller number of parameters decreases the iterations required to reach equilibrium, as well as the computation time.

From the reduced model, the betatron tune is systematically higher than that from the original model, due to the term  $A(j)$  in the original model shifting the sinusoidal frequency. The average tune difference of all BPMs is as small as  $1.7 \times 10^{-6}$ , which is sufficiently small for almost any real application. What is more important is the difference of the inferred optics, which is uncertainly between two models.

Figure 9 shows the comparison of the inferred beta function of the reduced model and the original model. With the reduced model (Eq. 7) we will have overlapped mean values of the beta function from the mean values of the original model, with about 0.4% standard deviation. However, the uncertainty of the beta function on average increases by about 4.4 times compared with the original model. The betatron phase advance of the reduced model also has larger uncertainties, ranging from 0.01 to 0.015 rad. They are about 5 times larger than that of the original model. The uncertainty of the optics function may play an important role in the lattice correction as pointed out in Ref [6]. The proper model should be selected based on the balance of requirements of precision and calculation time.

For the factor  $A(j)$ , it is also worthwhile to note that the choice of the quadrature form  $\exp(-\epsilon_{SR}j - \epsilon_{NL}^2 j^2)$  is not arbitrary. On one hand, we understand that these two terms have their physics meaning. On the other hand, we may also get a hint only from the BPM data pretending that we do not have accelerator physics knowledge. If  $A(j)$  only has the form of the exponential decay term:

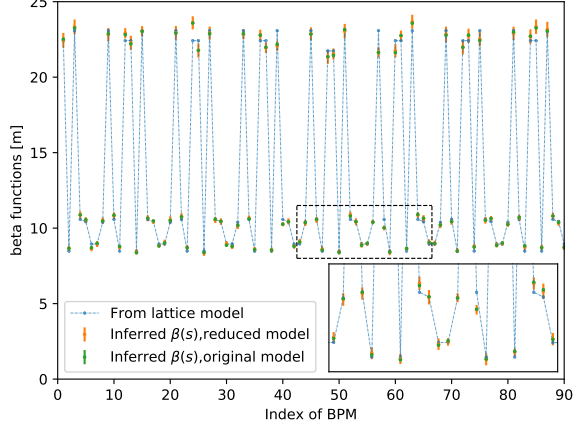


Figure 9. The inferred beta function at first 90 BPMs with the original and reduced model.

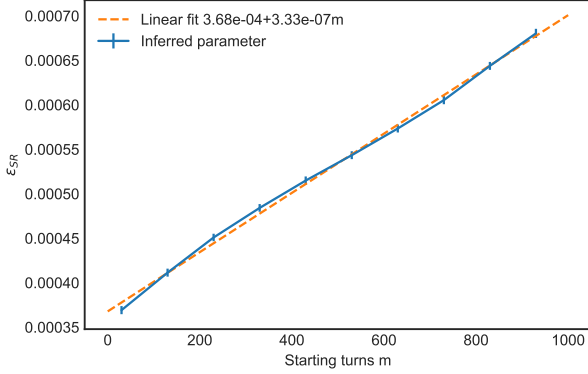


Figure 10. The inferred  $\epsilon_{SR}$  from 1000 turns data with varying starting turns.

$$A(j) = A(0) \exp(-\epsilon_{SR}j)$$

where  $A(0) = 1$ . The envelope decay would be 'memoryless', viz. we expect the same parameter  $\epsilon_{SR}$ , no matter from which turns we start our analysis. If we start our analysis from  $m^{\text{th}}$  turn:

$$\begin{aligned} A(j+m) &= A(0) \exp(-\epsilon_{SR}(j+m)) \\ &= A(0) \exp(-\epsilon_{SR}m) \exp(-\epsilon_{SR}j) \\ &= A(m) \exp(-\epsilon_{SR}j) \end{aligned}$$

We can test by select 1000 turns portion of data out of the 2000 turn with varying starting turns and use them with the model which contains  $A(j) = \exp(-\epsilon_{SR}j)$  and found that the inferred  $\epsilon_{SR}$  is not a constant, as shown in Figure 10

Instead of a flat dependence, the inferred  $\epsilon_{SR}$  has a significant slope as function of the starting turn  $m$ . There-

fore, it is expected that extra terms should be used in  $A(j)$ :

$$A(j) = A(0) \exp(-\epsilon_{SR}j + f(j))$$

If the inference process starts from turn  $m$  and the function  $f$  satisfy

$$f(j+m) = f(j) + f(m) + \kappa mj \quad (8)$$

we have:.

$$\begin{aligned} A(j+m) &= A(0) \exp(-\epsilon_{SR}(j+m) + f(j+m)) \\ &= A(m) \exp(-(\epsilon_{SR} + \kappa m)j + f(j)) \end{aligned}$$

where the term  $\kappa m$  is the feed-down effect of function  $f$ . Clearly, the function  $f$  with quadrature form satisfies the relation Eq.8. Therefore, learning from the data, we may conclude that a quadrature term in  $A(j)$  will better reflect the model.

Our model (as in Eq.5) will not reflect the all physics hidden in the data. Figure 5 indicates that there are still signals in the difference between the data and the model. It is easy to identify the synchrotron sidebands and the transverse coupling as stated in the previous sections. If these information is needed, a more precise model can be adopted. For instance, we can extend the model to extract the chromatic decoherence, by modifying the decoherence term  $A(j)$  as:

$$A(j) = \exp\left(-\epsilon_{SR}j - \epsilon_{NL}^2 j^2 - \frac{\alpha^2(j) - \alpha^2(0)}{2}\right)$$

with the new function  $\alpha(j)$  has the form:

$$\alpha(j) = \frac{2\xi_x \sigma_E}{\nu_s} \sin(\pi\nu_s j + \phi_s)$$

which is representing the chromaticity decoherence [8].  $\xi_x$  is the linear chromaticity of  $x$  direction,  $\sigma_E$  is the rms energy spread,  $\nu_s$  is the synchrotron tune and  $\phi_s$  is the synchrotron phase. Using this synchro-beta model, three more parameters can be extracted, which are  $\epsilon_E = \xi_x \sigma_E$ ,  $\nu_s$  and  $\phi_s$ , in addition to the parameters  $\theta = (x_0, x_c, P_x, \nu_x, \epsilon_{SR}, \epsilon_{NL})$  in the original model. Based on the fact that the synchro-betatron mode is a small perturbation of the betatron motion, the mean values of the inference results from the original model can be used as the prior information to infer the synchro-betatron parameters. Figure 11 demonstrates that inference results of the BPM #9. The product  $\xi_x \delta_E$  saturates at  $1.9 \times 10^{-3}$  with standard deviation of  $0.02 \times 10^{-3}$ . This is consistent with estimated chromaticity  $\sim 2$  and rms energy spread of  $\sim 9 \times 10^{-4}$ . The inferred synchrotron tune also meets the values from the lattice model. The minimization of the model and the data is a weaker function of the synchrotron phase, therefore the synchrotron phase has a large standard deviation from its inferred value.

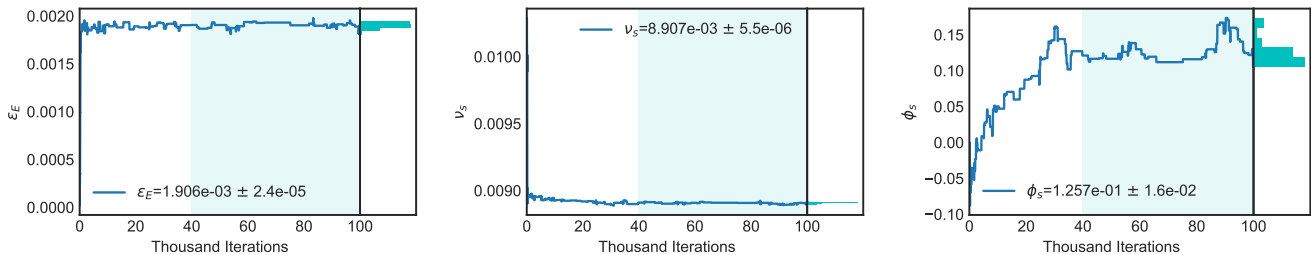


Figure 11. The inference of the synchrotron oscillation parameters Left:  $\epsilon_E = \xi\sigma_E$ , middle:  $\nu_s$  right: synchrotron phase  $\phi_s$ .

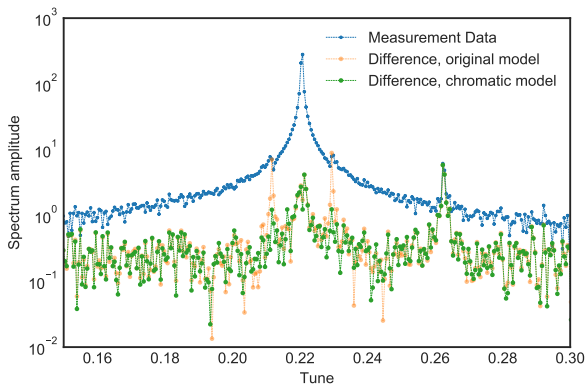


Figure 12. The frequency spectrum of the measurement data of BPM #9 and the difference between measurement and model with inferred parameters, with the original model (orange dots) and the model with chromatic decoherence (green dots)

Figure 12 demonstrates that after using the chromatic decoherence term in  $A(j)$ , we can eliminate the two synchrotron side band from the frequency spectrum of the difference of the measurement and the model.

However, we only successfully extract the information from the data of part of the BPMs. For more than half of the BPMs (for example BPM #1), the inferred synchrotron tune saturates at twice of the synchrotron values tunes. This issue may related to the fact that the chromatic decoherence is a weak signal compared with the betatron motions, and requires further investigations.

## SUMMARY

In this paper, we introduce a new approach of using the measurement data to infer the parameters of the accelerator model, using MCMC based Bayesian Inference. It requires our prior knowledges, which include a proper accelerator model with parameters to be determined and our belief (prior distribution) on the parameters. The MCMC algorithm used in Bayesian Inference can generate the samples of the posterior distribution of the un-

known parameters in the model using only single snapshot of measurement data. From the samples, the most probable values of the parameters and their standard deviation are obtained. Using Bayesian approach, multiple data requisition is not necessary. Therefore pollution due to the slow drift of machine parameters and the environment is mitigated or significantly reduced. In addition, the model can be extended or refined, both from the accelerator physics knowledges and from the data analysis. If the model extension is expected to be a perturbation, the posterior distribution of origin model can serve as the prior distribution of the extended one.

A proof-of-principle example is demonstrated by exploring the inference of optics functions of the betatron motion in horizontal plane, using measurement data of the NSLS-II electron storage ring. There is no foreseen difficulty to apply the method to hadron rings. A direct application of the reconstructed optics functions is the optics correction. As pointed out in Ref [6], the statistical properties of the optics function will gain more insight in the optics correction process by avoiding over-fitting. With different model used, this approach could also be potentially extended to analyzing more complicated dynamics in accelerators, such as determining coupling, analyzing the nonlinear dynamics properties, or estimate the reliability of the each instrumentation devices.

## ACKNOWLEDGMENTS

Work supported by the National Science Foundation under Cooperative Agreement PHY-1102511, the State of Michigan and Michigan State University. This research also used resources of the National Synchrotron Light Source II, a U.S. Department of Energy (DOE) Office of Science User Facility operated for the DOE Office of Science by Brookhaven National Laboratory under Contract No. de-sc0012704.

## APPENDIX: MARKOV CHAIN MONTE-CARLO METHOD

Markov Chain Monte-Carlo (MCMC) is a powerful method, which can sample the posterior distribution of



the parameters of interest. It is especially useful when in Bayesian Inference case (Eq.1), since the marginal distribution  $P(M)$  is usually impossible to be directly calculated. The MCMC method constructs a Markov chain, whose equilibrium distribution is proportional to the product of the likelihood and prior distribution, and sample it using Monte-Carlo method. The details of MCMC can be found in many text books, such as Chapter 10 in Ref [11]. Here we only outline the algorithm of MCMC used this article.

We use the Hastings-Metropolis algorithm, an MCMC algorithm, to get the sample of random variable  $\theta^i$ , with  $i$  as the iteration index, whose limiting probability is the posterior distribution  $P(\theta | M)$ . The algorithm is detailed as below procedures:

1. Choose initial condition ( $0^{\text{th}}$  iteration)  $\theta^0$ . The choice does not affect the inference result. However, a reasonable guess of the initial condition reduces the required iteration to reach equilibrium.

2. Evaluate the  $\pi(i) = P(M | \theta^i) \cdot P(\theta^i)$  for the  $i^{\text{th}}$  iteration
3. Make Gaussian random walk centered at the value of  $\theta^i$ , with preset step size as the standard deviation, to get the new trial parameters  $\theta^t$
4. Evaluate the  $\pi(t) = P(M | \theta^t) \cdot P(\theta^t)$
5. Get a sample  $u$  from uniform random distribution  $[0, 1]$
6. If  $u < \min\left(\frac{\pi(t)}{\pi(i)}, 1\right)$ , the random walk is accepted,  $\theta^{i+1} = \theta^t$ ; otherwise  $\theta^{i+1} = \theta^i$

We continue this procedure for  $N$  iterations. If after first  $n (< N)$  iterations, the chain reaches its equilibrium, then the sequence  $(\theta^{n+1}, \theta^{n+2}, \dots, \theta^N)$  is the desired sampling of the posterior distribution of  $\theta$ .

- 
- [1] R. Tomás, M. Aiba, A. Franchi, and U. Iriso, Phys. Rev. Accel. Beams **20**, 054801 (2017).
- [2] X. Huang, S. Y. Lee, E. Prebys, and R. Tomlin, Phys. Rev. ST Accel. Beams **8**, 064001 (2005).
- [3] J. Irwin, C. X. Wang, Y. T. Yan, K. L. F. Bane, Y. Cai, F.-J. Decker, M. G. Minty, G. V. Stupakov, and F. Zimmermann, Phys. Rev. Lett. **82**, 1684 (1999).
- [4] P. Castro-Garcia, *Luminosity and beta function measurement at the electron - positron collider ring LEP*, Ph.D. thesis, CERN (1996).
- [5] J. Safranek, Nuclear Instruments and Methods in Physics Research Section A: Accelerators, Spectrometers, Detectors and Associated Equipment **388**, 27 (1997).
- [6] Y. Li, R. Rainer, and W. Cheng, Phys. Rev. Accel. Beams **22**, 012804 (2019).
- [7] Y. Li, W. Cheng, K. Ha, and R. Rainer, Phys. Rev. Accel. Beams **20**, 112802 (2017).
- [8] R. E. Meller, A. W. Chao, J. M. Peterson, S. G. Peggs, and M. Furman, SSC-N-360 (1987).
- [9] BNL, <https://www.bnl.gov/ns1s2/project/PDR/>.
- [10] J. Laskar, C. Froeschlé, and A. Celletti, Physica D: Nonlinear Phenomena **56**, 253 (1992).
- [11] S. M. Ross, *Simulation (4.th ed.)* (Elsevier, 2006).